Supporting Information for

Molecular Origins of the Nonlinear Optical Response of a Series of α-(X-2-Pyridylamino)-*O*-Cresol Chromophores from Concerted X-ray Diffraction, Hyper-Rayleigh Scattering, and *Ab Initio* Calculations

Christopher M. Ashcroft,[1] Jacqueline M. Cole,[1,2,3,4,*] Edward A. Boardman[1] Tze-Chia Lin,[1] Javier Perez-Moreno,[5,6] Koen Clays[5]

[1] *Cavendish Laboratory, Department of Physics, University of Cambridge, J. J. Thomson Avenue, Cambridge, CB3 0HE, UK*

[2] *ISIS Neutron and Muon Source, STFC Rutherford Appleton Laboratory, Harwell Science and Innovation Campus, Didcot, Oxfordshire, OX11 0QX, UK*

[3] *Department of Chemical Engineering and Biotechnology, University of Cambridge, West Cambridge Site, Philippa Fawcett Drive, Cambridge, CB3 0AS, UK*

[4] *Argonne National Laboratory, 9700 S. Cass Avenue, Argonne, IL 60439, USA*

[5] *Department of Chemistry, University of Leuven, Celestijnenlaan 200D, 3001 Leuven, Belgium*

[6] *Department of Physics, Skidmore College, 815 N Broadway, Saratoga Springs, NY 12866, USA*

* Email for correspondence: jmc61@cam.ac.uk

Table of Contents

S.1 X-ray Wave-Function Refinement (XWR) Fit S3

*S.1.1 XWR λ_L vs. χ^2 Graphs for **1-3*** S3

*S.1.2 XWR QQ Plots for **1-3*** S3

*S.1.3 XWR Scatter Plots for **1-3*** S5

*S.1.4 XWR Residual Electron Density Maps for **1-3*** S7

S.2 XWR-derived QTAIM Analysis S9

*S.2.1 QTAIM Parameters of **2*** S9

*S.2.2 QTAIM Parameters of **3*** S10

*S.2.3 Electron Deformation Density maps of **1-3*** S13

S.3 Solution State UV/Vis Absorption Spectroscopy of **1-3** S15

S.4 References S17

S.1 X-ray Wave-Function Refinement (XWR) Fit

Herein, λ_L *vs.* χ^2 *graphs,* normal probability distribution (Q-Q) plots, scatter plots, and residual electron density maps of the XWR fits of **1-3** are presented in order to assess the quality of each XWR fit.

S.1.1 XWR λ_L *vs.* χ^2 *graphs for* ***1-3***

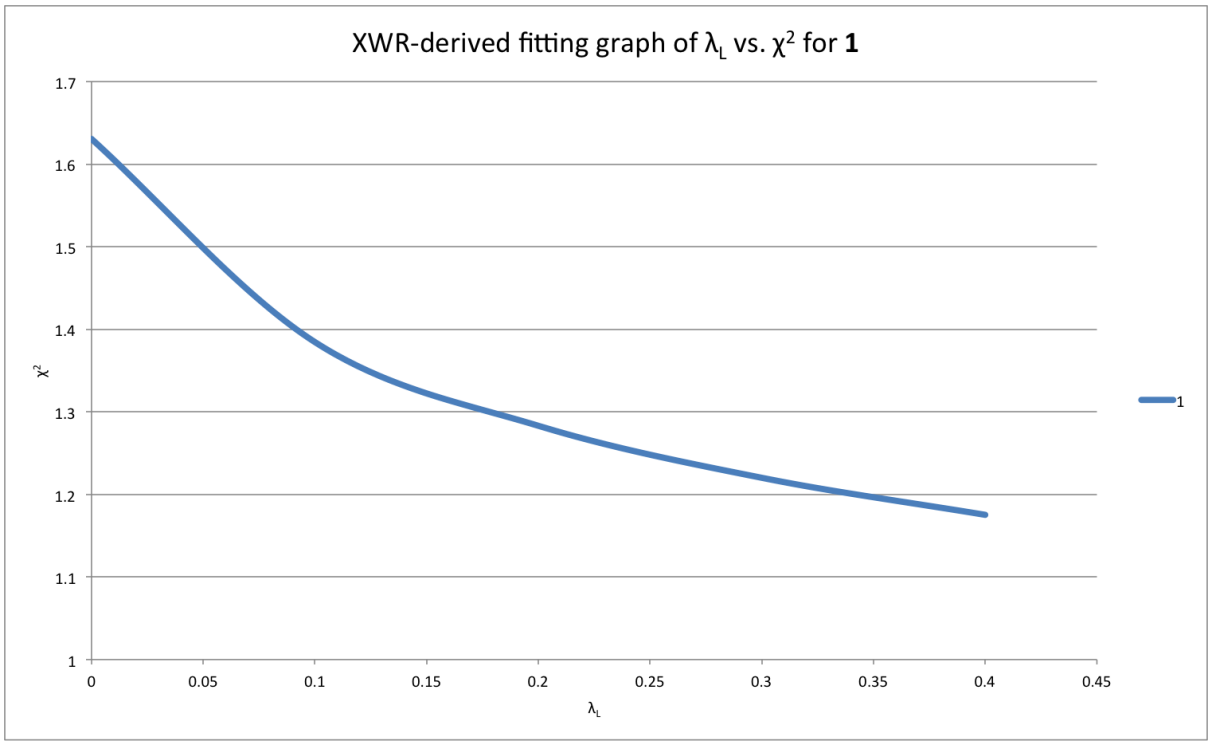

Figure S1 $\boldsymbol{\lambda_L}$ vs. $\boldsymbol{\chi^2}$ fitting graph for **1**.

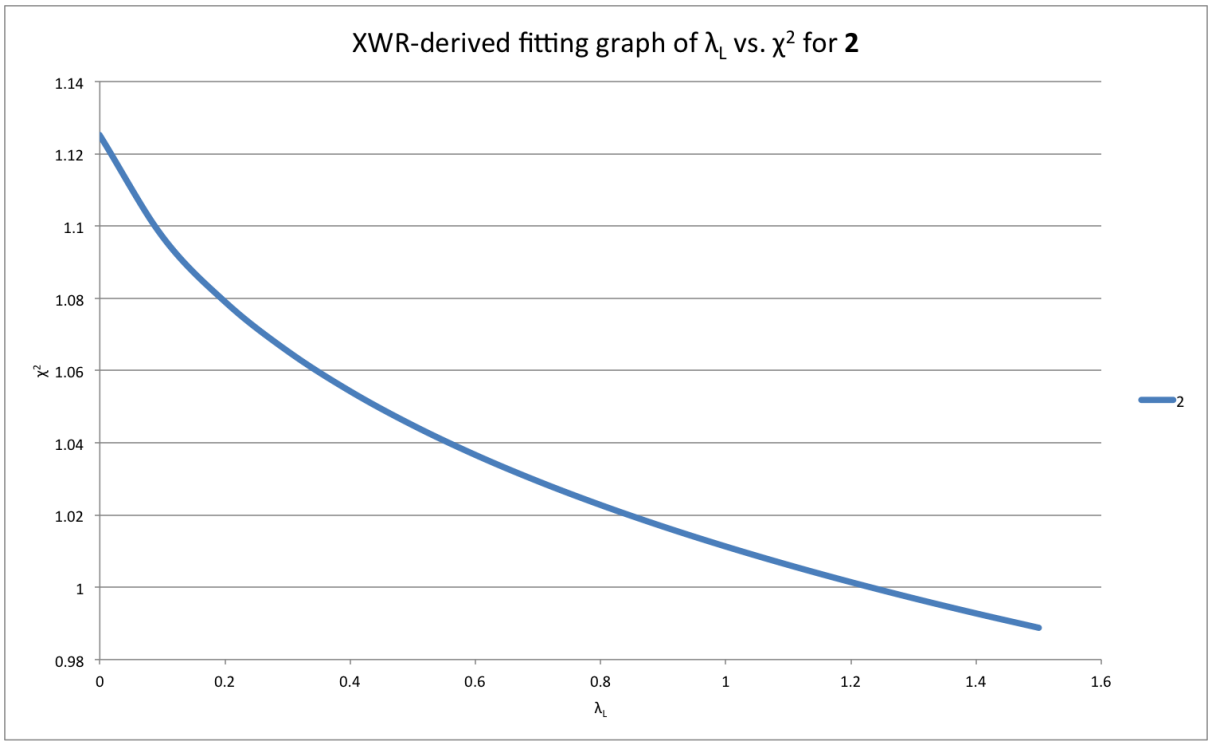

Figure S1 λ_L vs. χ^2 fitting graph for **2**.

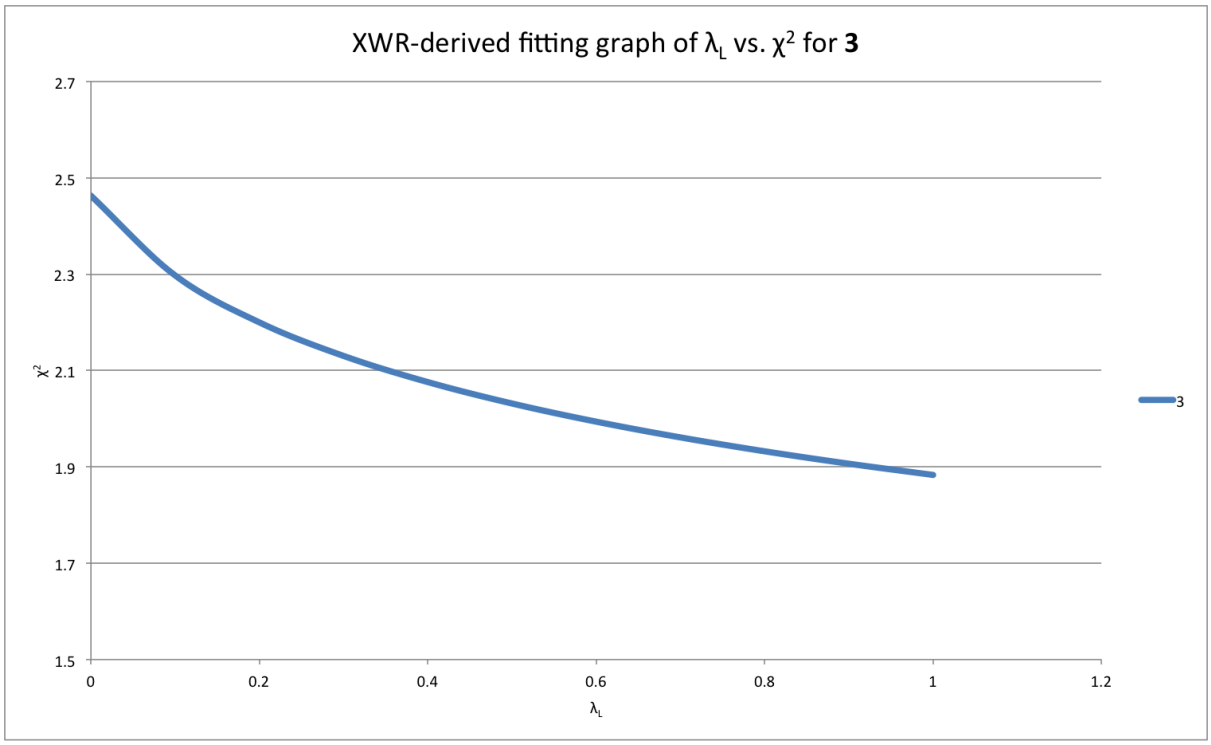

Figure S1 λ_L vs. χ^2 fitting graph for **3**.

*S.1.2 XWR Q-Q Plots for **1-3***

Q-Q plots are probability plots that compare theoretical with the experimental data quantiles,[1] whereby a perfect fit corresponds to the data lying along the line y = x. All three Q-Q plots (Fig S4-S6) exhibit a divergence from a Gaussian distribution for the tails of the distributions, which likely corresponds to problems modeling strong low-angle reflections; while the middle regions of the plots replicate a normal distribution well. R^2 values for each plot are shown for comparison.

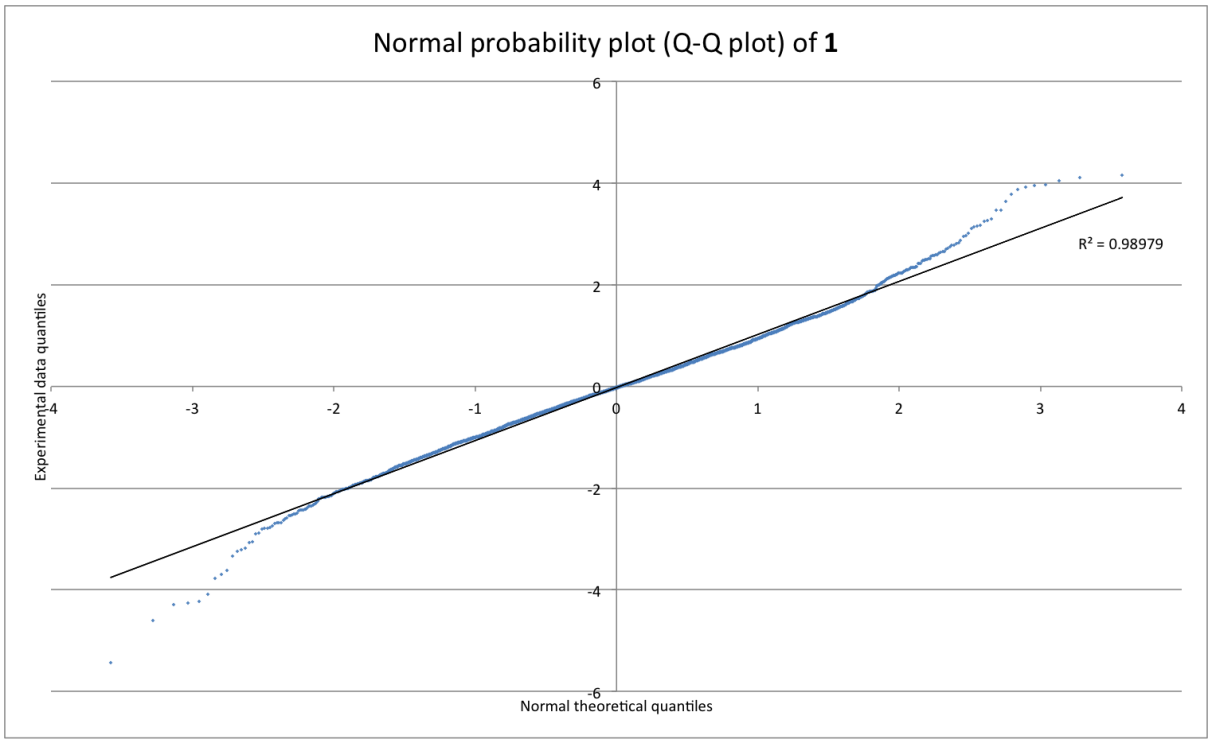

Figure S4 Normal probability plot (Q-Q plot) for **1**.

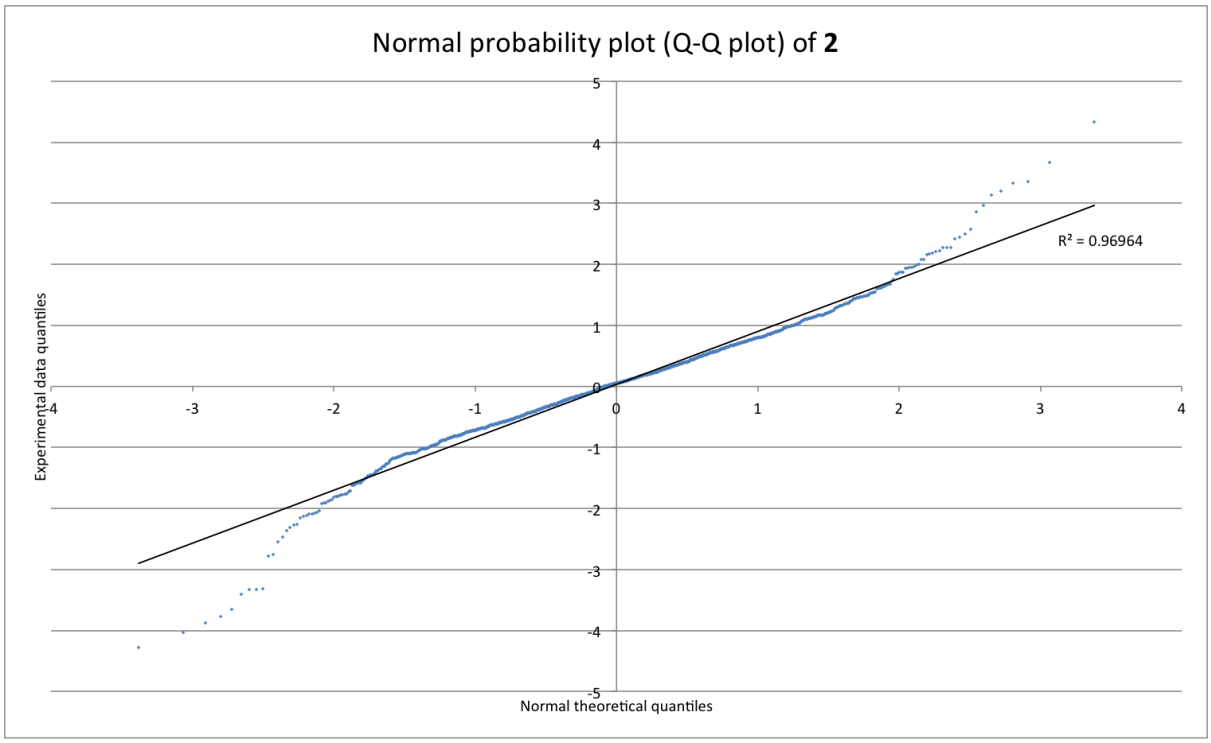

Figure S5 Normal probability plot (Q-Q plot) for **2**.

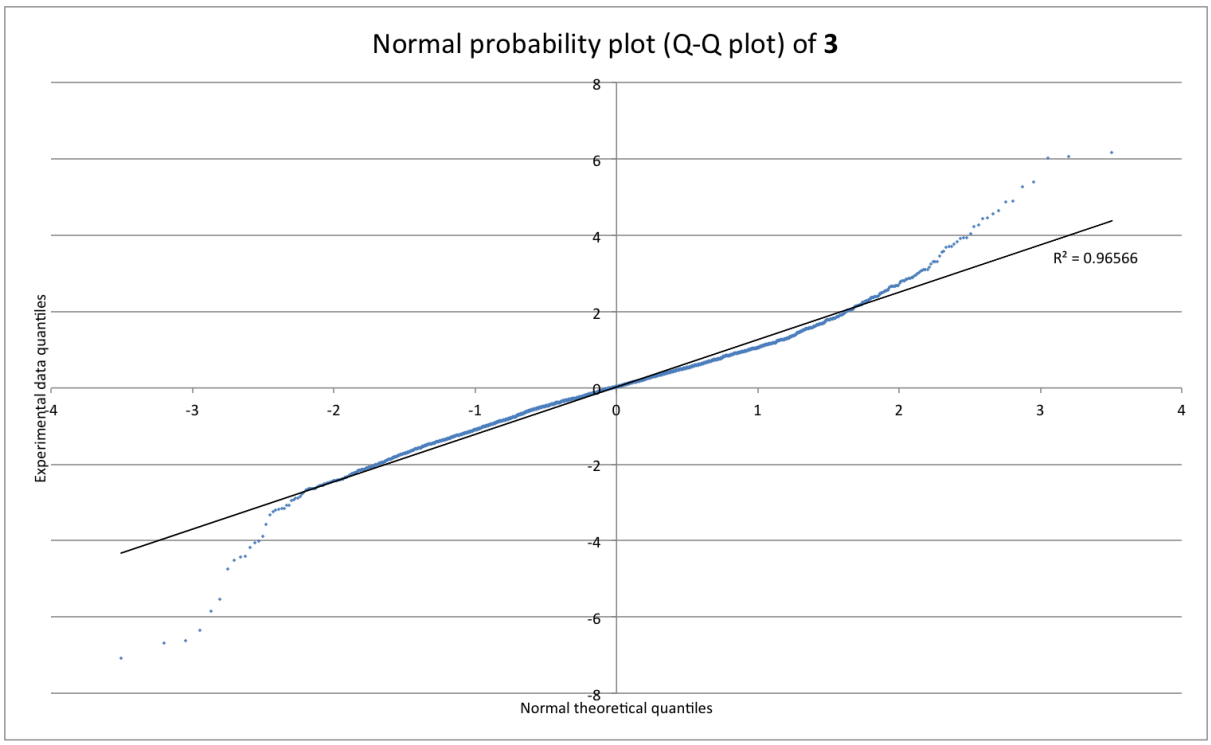

Figure S6 Normal probability plot (Q-Q plot) for **3**.

*S.1.3 XWR Scatter Plots for **1-3***

Scatter plots of the residuals of F_z vs. $sin(\vartheta)/\lambda$ (where F_z is defined by Eq. S1) of **1-3** were generated (Fig S7-S9) and reveal how well reflections are being modeled. For a good fit/model, these plots should be uniform and show a symmetrical distribution of data points along the line y = 0.

$$F_z = \frac{(F_{obs} - F_{calc})}{\sigma(F_{obs})} \qquad \text{(S1)}$$

All three plots exhibit a symmetrical distribution for the majority of the data points, whereby **1** show the most uniform distribution. The plots for **2** and **3** show some divergence from a symmetrical distribution, whereby **2** shows the highest divergence. This divergence may be a consequence of incorrect estimations of the errors of these data points. A comparison of the residual scatter plots for **1-3** with their analogous Q-Q plots (*cf.* §S1.2) indicates that errors associated with data points in the tails of the distributions are underestimated. The effect of incorrect estimations of the standard errors of reflections has already been discussed.[2]

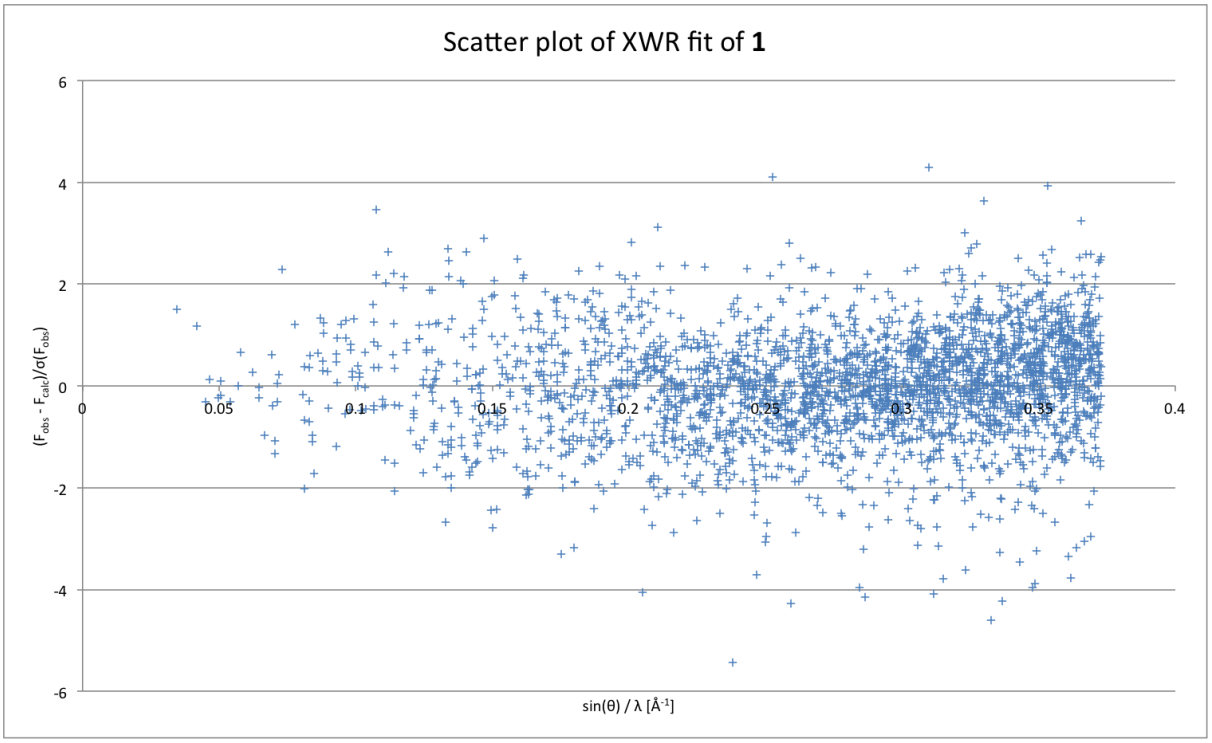

Figure S7 Scatter plot of the residuals of **1** following convergence of the XWR fit .

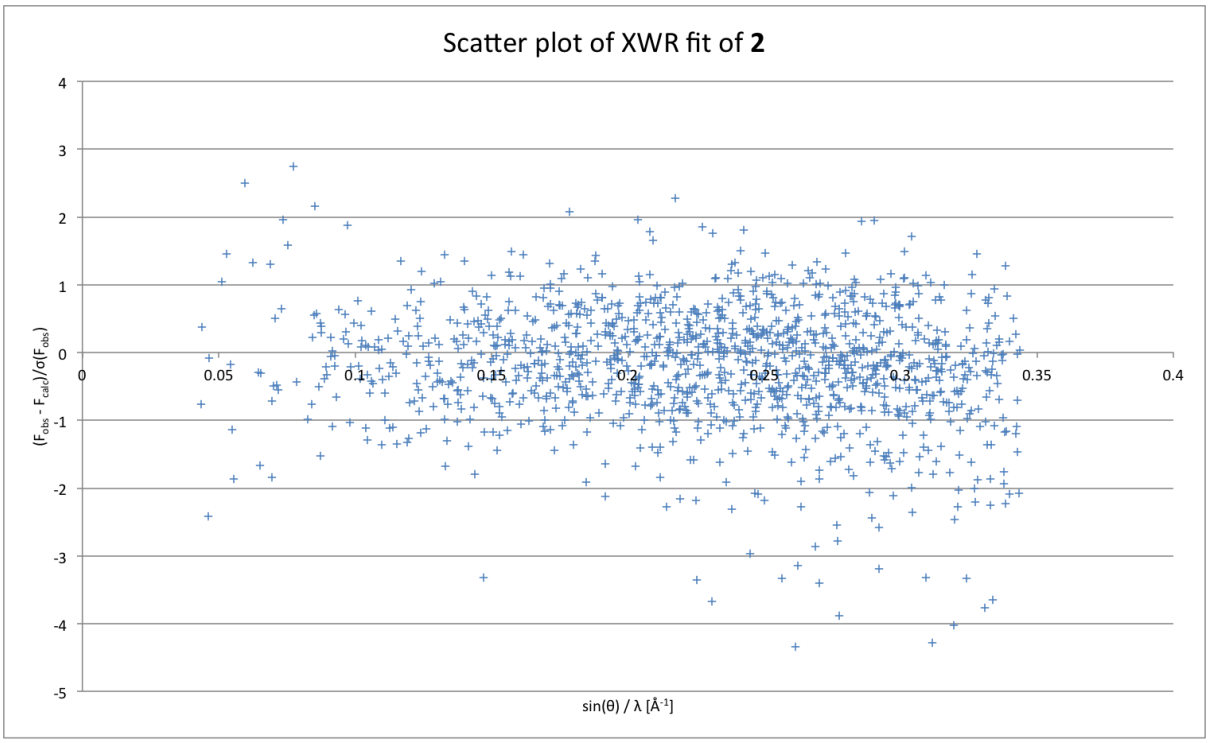

Figure S8 Scatter plot of the residuals of **2** following convergence of the XWR fit.

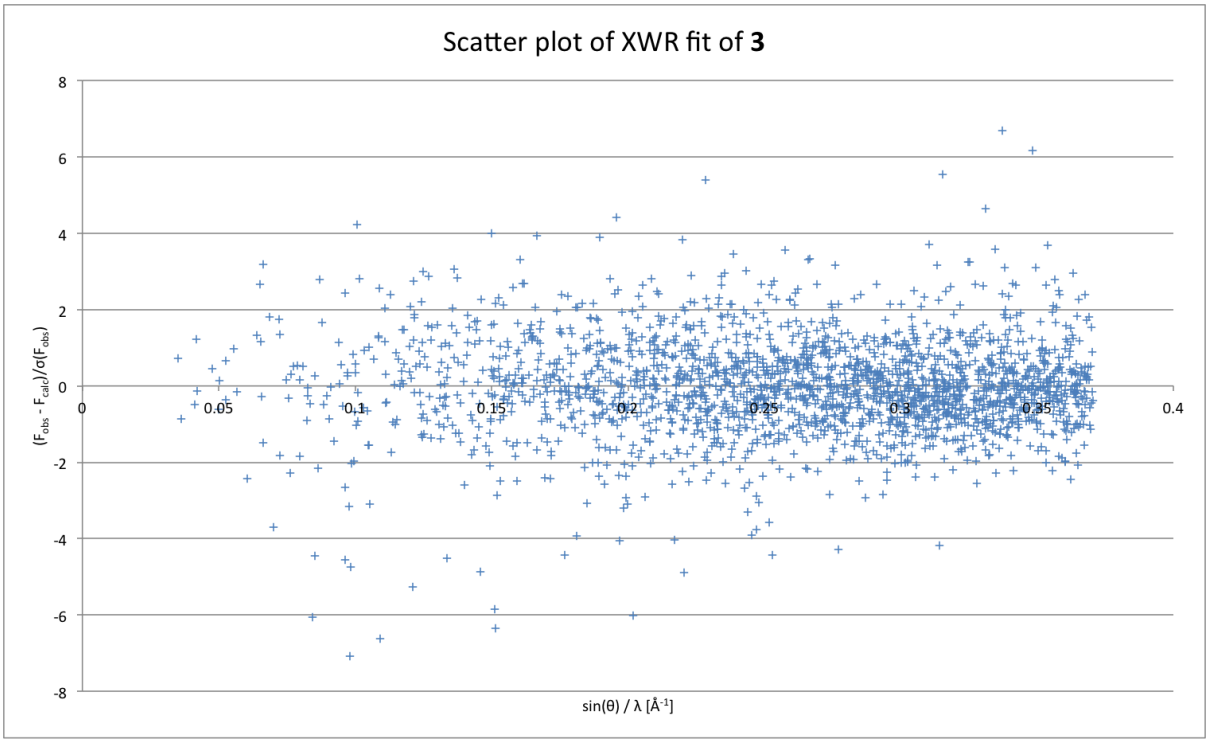

Figure S9 Scatter plot of the residuals of **3** following convergence of the XWR fit.

*S.1.3 XWR Residual Electron Density Maps for **1-3***

Residual electron density maps for **1-3** are presented in Fig S10; red lines represent positive electron density, while blue lines represent negative electron density, and black lines represent zero electron density (contour levels = 0.1 eÅ^{-3}). An ideal residual electron density plot would be flat; while areas that contain residual electron density correspond to regions that are not completely modeled.

The residual electron density map of **1** is flat and featureless except for a few small residual density features that appear to be randomly distributed and which cannot be attributed to any specific segments or atoms within the molecule.

The residual electron density maps for **2** and **3** appear somewhat more featured compared to that of **1**. That said, most of those features are randomly distributed and cannot be attributed to unmodeled bonding or lone-pair phenomena, except for the terminal Cl atoms. In the case of the Cl atoms, residual electron density is observed in the residual electron density maps of **2** and **3** either within the bonding region or, at the position of the Cl atom itself. Nevertheless, the residual electron density residing on the Cl atom of **2** is small (0.13 eÅ^{-3}). In the case of **3**, the unmodeled residual density of the two Cl atoms is higher (0.24 eÅ^{-3}) which is nevertheless still modest; and, it appears to have a shashlik character, which can be a sign of anharmonic libration of the atom. The presence of such anharmonic libration is not surprising given the terminal position of the Cl atoms. Owing to the absence of high resolution data, a Gram-Charlier (GC) anharmonic refinement of **3** could not be undertaken.[3] As a consequence of this unmodeled 0.24 eÅ^{-3} residual electron density, care was taken when assessing the viability of the model of **3** and its associated determined properties. The fitting statistics for **3** are nevertheless acceptable (*cf.* §2.3) and the bonding parameters associated with the Cl atoms are reasonable (*cf.* §3.2.2; Table 4) as were their respective Laplacian maps (*cf.* §3.2.2; Fig 4 & 5).

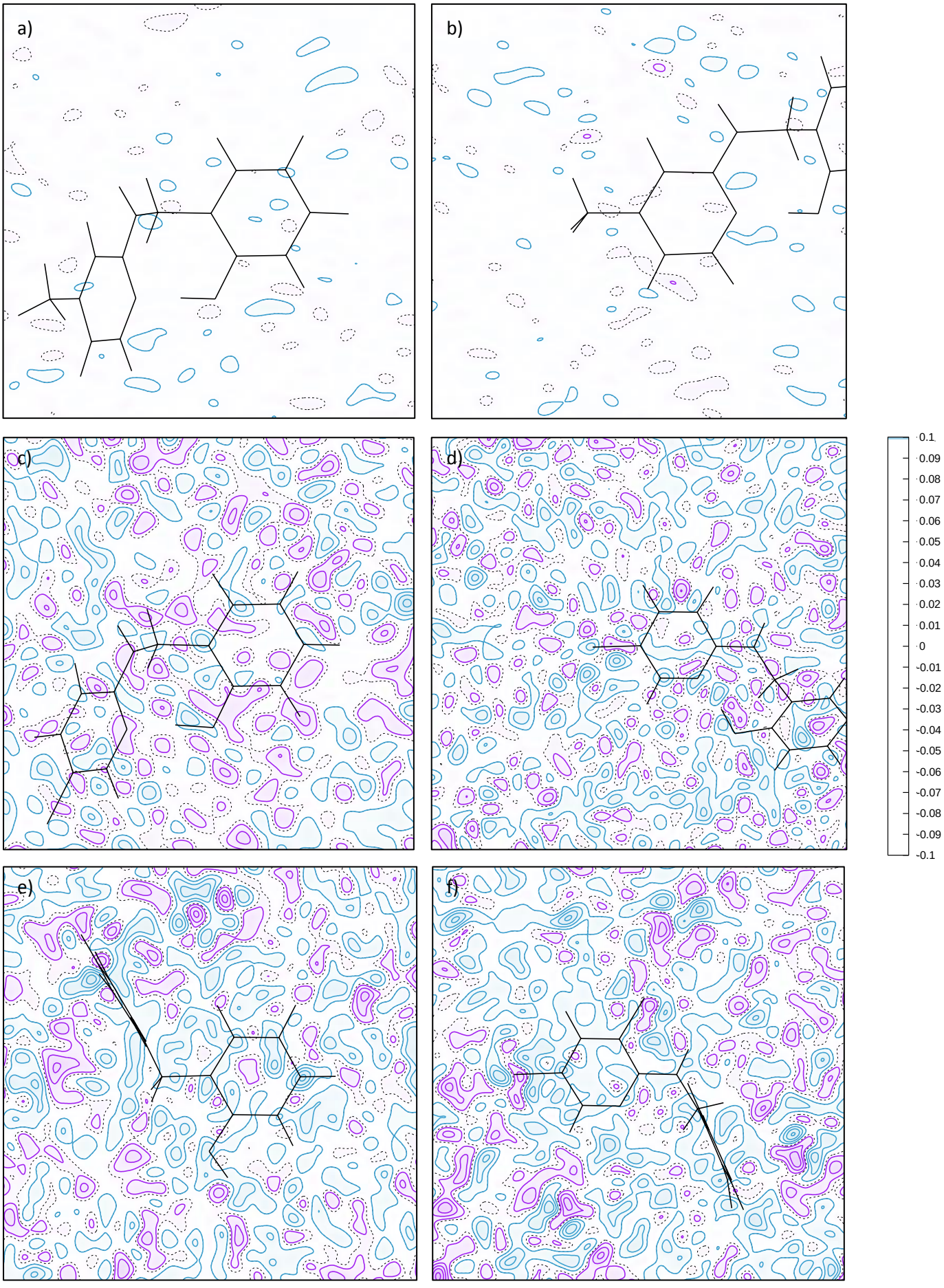

Figure S10 Residual electron density maps for **1** (a-b), **2** (c-d), and **3** (e-f) (contour level: 0.1 eÅ^{-3}).

S.2 XWR-derived QTAIM Analysis

The QTAIM bonding parameters for **2** and **3** are shown in Table S1 and S2, respectively.

Bond	ρ(r)	$\nabla^2\rho$(r)	ε	G(r)/ρ(r)	H(r)	Bond type *cf.* Table 2.
C1-C2	2.121	-21.422	0.32	0.305	-0.318	Covalent (π)
C2-C3	2.158	-24.732	0.07	0.223	-0.328	Covalent (σ/π)
C3-C4	2.198	-14.586	0.10	1.234	-0.553	Polar shared (π)
C4-C5	2.197	-24.325	0.19	0.267	-0.339	Covalent (π)
C5-C6	2.153	-26.009	0.08	0.221	-0.340	Covalent (π)
C6-C1	2.184	-26.721	0.03	0.194	-0.340	Covalent (σ)
C6-O	2.061	-14.540	0.09	1.135	-0.498	Polar shared (π)
C1-C7	1.774	-17.652	0.01	0.188	-0.232	Covalent (σ)
C7-N1	1.722	-11.960	0.07	1.027	-0.386	Polar shared (σ/π)
N1-C8	2.187	-21.922	0.01	0.985	-0.547	Covalent (σ)
C8-N2	2.358	-25.603	0.09	0.975	-0.606	Covalent (π)
N2-C9	2.198	-14.586	0.10	1.234	-0.553	Polar shared (π)
C9-C10	2.257	-24.820	0.28	0.287	-0.354	Covalent (π)
C10-C11	2.119	-21.581	0.26	0.289	-0.315	Covalent (π)
C11-C12	2.220	-23.691	0.23	0.301	-0.345	Covalent (π)
C12-C8	2.108	-22.805	0.19	0.270	-0.321	Covalent (π)
C10-Cl1	1.397	-9.947	0.05	0.327	-0.171	Covalent (σ)
H Bond (N2---H1)	0.479	2.378	0.05	0.723	-0.027	Mixed

Table S1. Parameters of the (3, -1) BCPs and intramolecular hydrogen-bond BCP of **2**. ρ(r) [eÅ^{-3}] is the electron density; $\nabla^2\rho$(r) [eÅ^{-5}] is the Laplacian of the electron density; ε is the ellipticity of the bond; G(r)/ρ(r) [a.u.] is the kinetic energy density per electron; H(r) [a.u.] is the energy density.

Bond	ρ(r)	$\nabla^2\rho$(r)	ε	G(r)/ρ(r)	H(r)	Bond type *cf.* Table 2.
C1-C2	2.124	-20.521	0.23	0.328	-0.316	Covalent (π)
C2-C3	2.081	-20.107	0.14	0.284	-0.296	Covalent (π)
C3-C4	2.173	-22.202	0.27	0.334	-0.338	Covalent (π)
C4-C5	2.164	-22.443	0.14	0.283	-0.324	Covalent (π)
C5-C6	2.172	-23.271	0.23	0.319	-0.344	Covalent (π)
C6-C1	2.156	-21.654	0.28	0.301	-0.321	Covalent (σ)
C6-O	1.942	-3.512	0.25	1.462	-0.457	Polar shared (π)
C1-C7	1.683	-14.757	0.06	0.212	-0.206	Covalent (σ)
C7-N1	1.793	-15.123	0.06	0.936	-0.406	Covalent (σ)
N1-C8	2.373	-33.849	0.09	0.608	-0.565	Covalent (σ/π)
C8-N2	2.369	-33.417	0.01	0.576	-0.549	Covalent (σ)
N2-C9	2.233	-15.679	0.08	1.208	-0.562	Polar shared (σ)
C9-C10	2.279	-26.777	0.07	0.250	-0.362	Covalent (σ)
C10-C11	2.124	-22.341	0.10	0.250	-0.310	Covalent (π)
C11-C12	2.232	-23.474	0.28	0.311	-0.346	Covalent (π)
C12-C8	2.136	-24.201	0.09	0.220	-0.321	Covalent (σ)
C10-Cl1	1.419	-9.815	0.06	0.314	-0.168	Covalent (σ)
C12-Cl2	1.431	-10.187	0.06	0.297	-0.169	Covalent (σ)

Table S2. Parameters of the (3, -1) BCPs and intramolecular hydrogen-bond BCP of **3.** ρ(r) [eÅ^{-3}] is the electron density; $\nabla^2\rho$(r) [eÅ^{-5}] is the Laplacian of the electron density; ε is the ellipticity of the bond; G(r)/ρ(r) [a.u.] is the kinetic energy density per electron; H(r) [a.u.] is the energy density.

S.2.3 Electron Deformation Density Maps of 1-3

Electron deformation density (EED) maps, derived from the XWR wavefunctions, for **1-3** are presented in Fig S11. Green lines represent areas with positive signum, while purple lines represent areas with negative signum, and dotted lines areas of zero (EDD). Contour levels are shown at 0.1 $eÅ^3$ linear scaling.

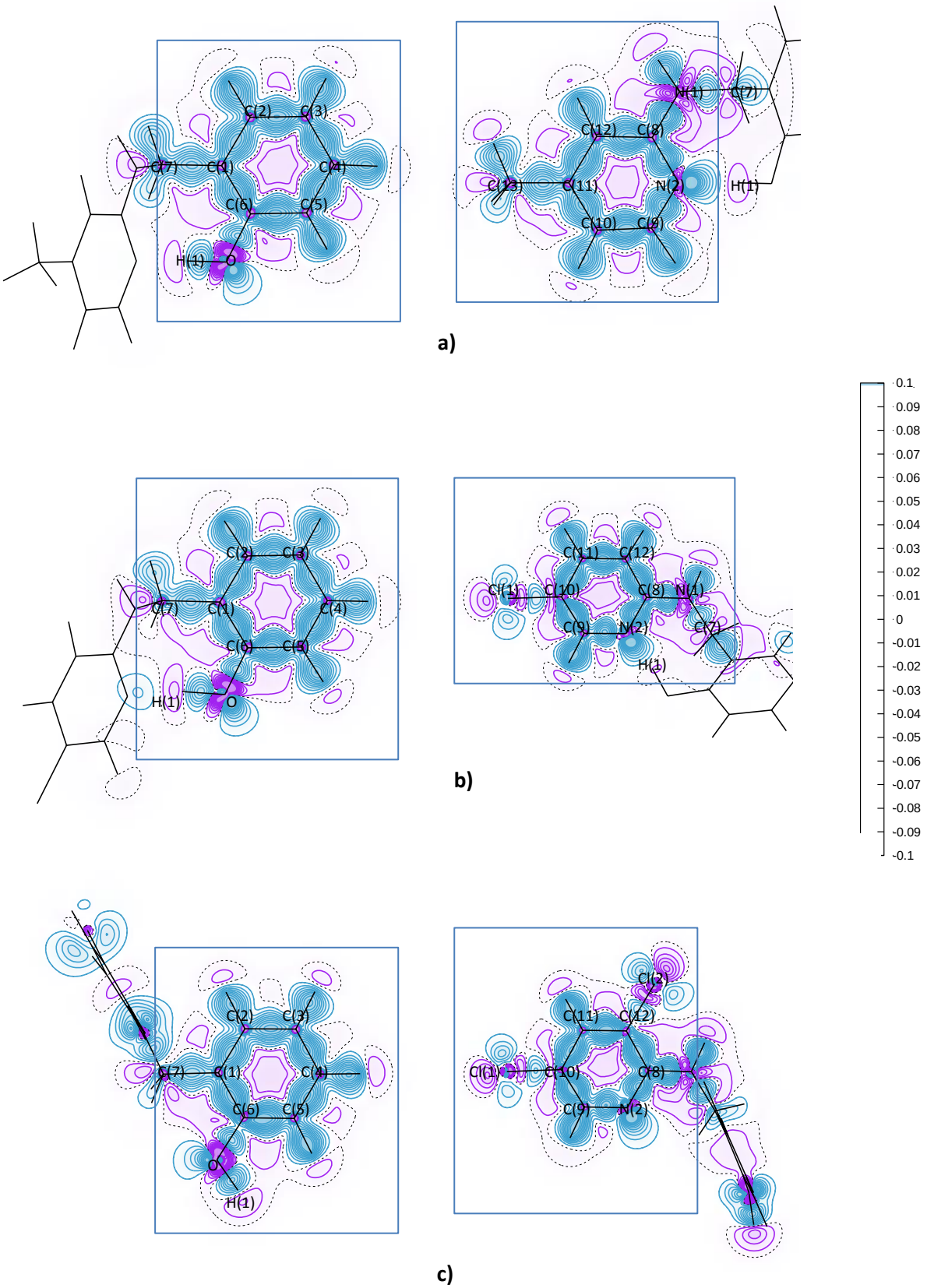

Figure S11. Electron deformation density (EDD) maps of (a) **1** (b) **2**, and (c) **3.** Boxed segments are in the plane of the page. Green lines represent areas with positive signum, while purple lines represent areas with negative signum, and dotted lines areas of zero (EDD). Contour levels are shown at 0.1 eÅ^{-3} linear scaling.

S.3 Solution State UV/Vis Absorption Spectroscopy of 1-3

UV/vis absorption spectra for **1** (1.27 mM), **2** (5.41 mM), and **3** (0.82mM) in acetone (Fig S8-S10) were recorded on an Agilent Cary 300 UV/vis spectrophotometer, and revealed the presence of absorption peaks just before the SHG wavelength (400 nm): 302nm (**1**), 317nm (**2**) and 328nm (**3**) . All spectra experience a wavelength cut-off at 300nm which, is indicative of the instrument cut-off of the spectrometer used in these measurements.

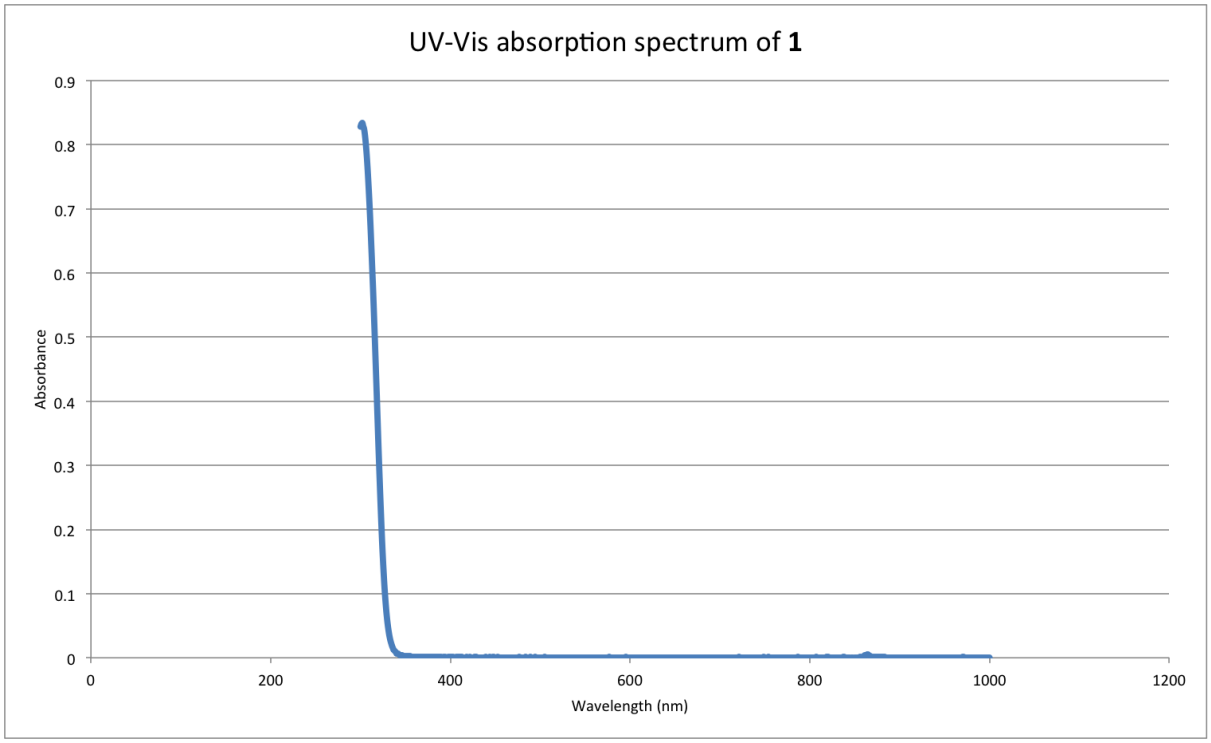

Figure S11 UV-Vis absorption spectrum of **1** in an acetone solution.

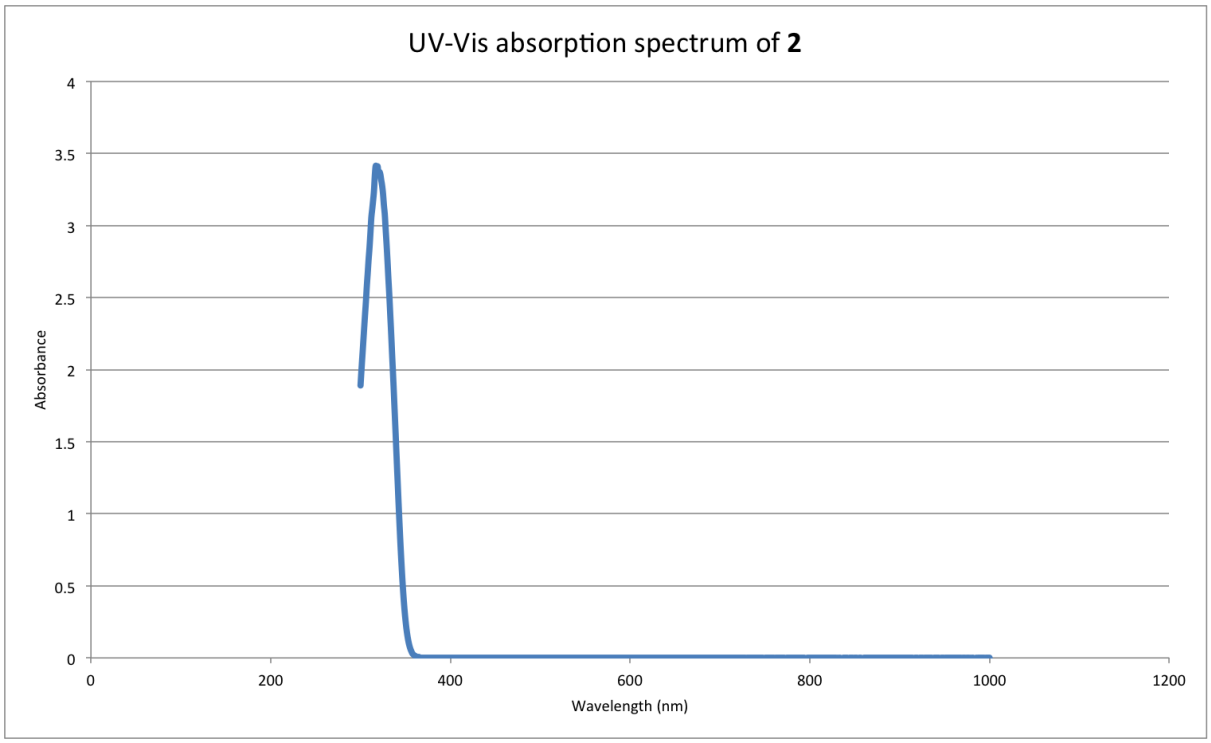

Figure S12 UV-Vis absorption spectrum of **2** in an acetone solution.

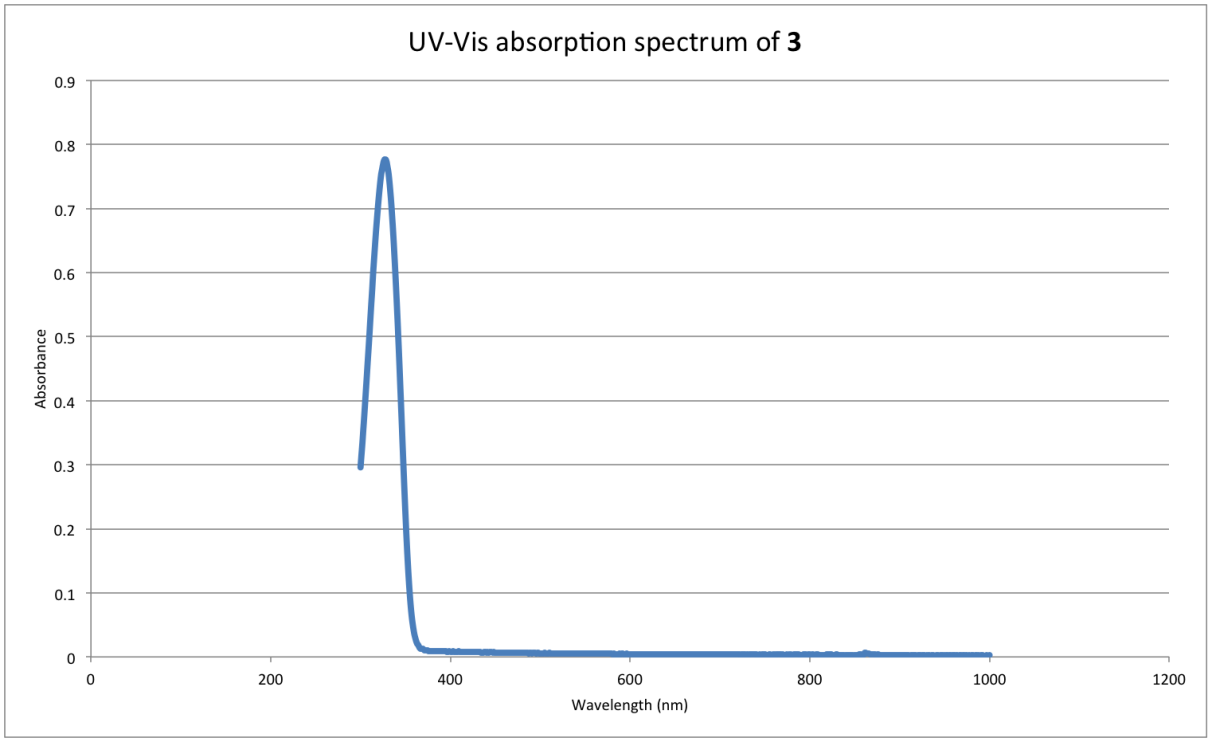

Figure S13 UV-Vis absorption spectrum of **3** in an acetone solution.

S.4 References

1. Abrahams, S. C. & Keve, E. T. Normal probability plot analysis of error in measured and derived quantities and standard deviations. *Acta Crystallogr. A* **27,** 157–165 (1971).
2. Henn, J. & Meindl, K. Two Common Sources of Systematic Errors in Charge Density Studies. *Int. J. Mater. Chem. Phys.* **1,** 417–430 (2016).
3. Kuhs, W. F. Generalized atomic displacements in crystallographic structure analysis. *Acta Crystallogr. A* **48,** 80–98 (1992).